Automated Ventriculargram Boundary Delineation

Robert M. Haralick, Jasjit Suri, Florence Sheehan

University of Washington
Seattle, WA 98195

Abstract. Quantitative analysis of the left ventricle wall motion is important for the diagnosis of coronary heart disease. From wall motion, stroke volume, ejection fraction, and velocity of ventricular circumference can be estimated. These are helpful in identifying the state of diseased hearts.
This paper describes a left ventricle boundary delineation algorithm which operates on X-Ray image data sets (ventriculargrams) produced in a catheterization laboratory for patient cardiovascular assessment. On a data set of 377 patient studies, the algorithm was able to delineate the boundary for the left ventricle with an average error just over 2.4 mm relative to the gold standard of cardiologist hand traced boundaries.

1 Ventriculography

Contrast ventriculography is a procedure routinely performed in clinical practice during cardiac catheterization. Catheters are intravascularly inserted into the heart to inject a contrast dye so that the left ventricle may be more clearly images with X-Rays. The time sequence of such image frames is called a ventriculogram. They constitute a projection image sequence of the endocardial surface of the left ventricle chamber. These images are used to determine the endocardial boundary at the end diastole, when the heart is filled up with blood, and at the end systole, when the heart is at the end of the contraction phase during the cardiac cycle.

A typical set of the end diastole and the end systole frames is shown in fig. 1. The left image shows the time frame when the left ventricle is filled with blood while the right image shows the time frame when the left ventricle is at the end of the contraction phase. By manually tracing the contour or boundary of the endocardial surface of the heart at these two extremes in the cardiac cycle, a cardiologist can determine the size and function of the left ventricle and can diagnose certain abnormalities or defects in the heart.

2 Characterstics of the Cardiac Data Sets

2.1 Variability in the Cardiac Data Sets

The variability in the cardiac data sets is to the heart rate, size, shape, position, orientation, and cardiac diseases like: ischemic cardiomyopathy, hypertensive

Fig. 1. Typical end distole and end systole frames of a cardiac cycle. **Left**: End distole frame, **Right**: End systole frame.

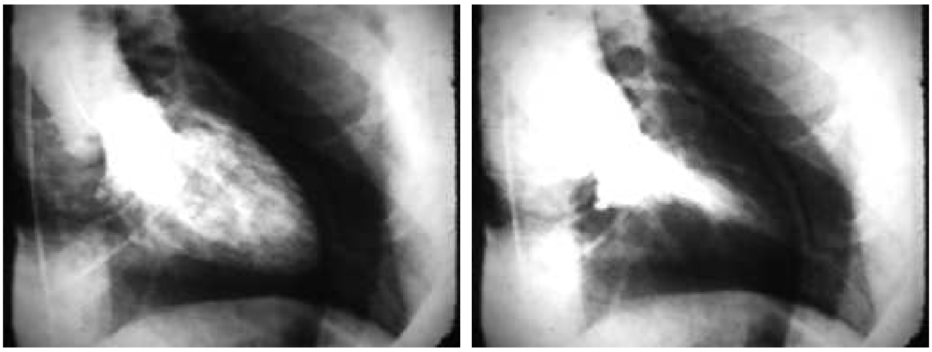

Fig. 2. Left: Position of catheter in the LV chamber. Also seen are the diaphragm and ribs. **Right**: Labelling of the LV parts: anterior wall, apex zone, inferior wall, aortic valve plane and the longitudinal axis.

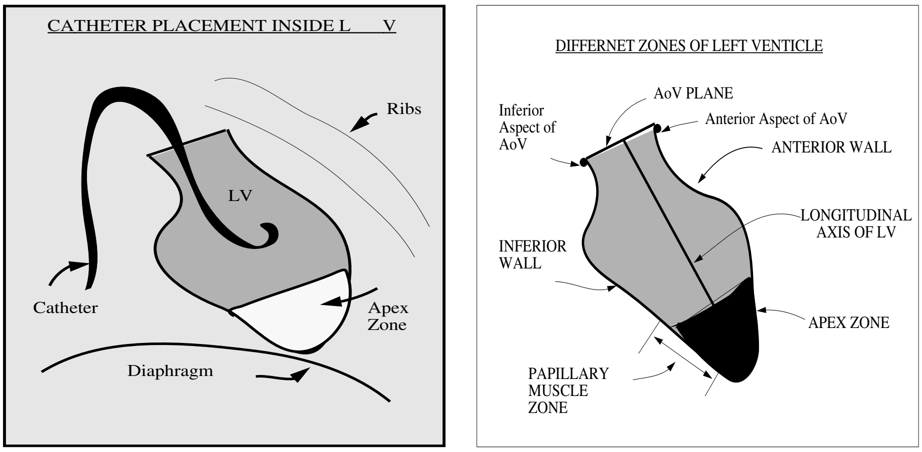

cardiomyopaothy, rheumatic heart disease, myocarditis, and congestive heart failure. Fig. 3 shows examples of the variability of the left ventricle shapes for the end diastole frame. Fig. 4 shows the variability of left ventricle shapes for the same studies as in fig. 3, but for the end systole frame. The bottom row shows two left ventricles having an altogether different orientation, position, size and shape for the end systole frame. The variability of left ventricle contrast during the systole cycle is shown in fig. 5.

One of the most serious shortcomings in these ventriculograms is the non-homogeneous mixing of the dye with the blood. This causes almost no propagation of the dye in the apical zone of the left ventricle chamber. Thus boundaries must be delineated in the apical zone where there may be no or little gray scale contrast across the boundary. The end systole apex position in end systole gray

Fig. 3. Demonstration of variability in the LV shapes in end diastole (ED) frame. LV image size: 384 x 512. **Top left:** LV has a bulge in the anterior wall. **Top right:** LVG has an almost horizontal inferior wall. **Bottom left:** The LV has a very different shape in the inferior wall zone. **Bottom right:** The LV is too tiny and bulge in the anterior wall. These different shapes demonstrate the large variability in cardiac data sets.

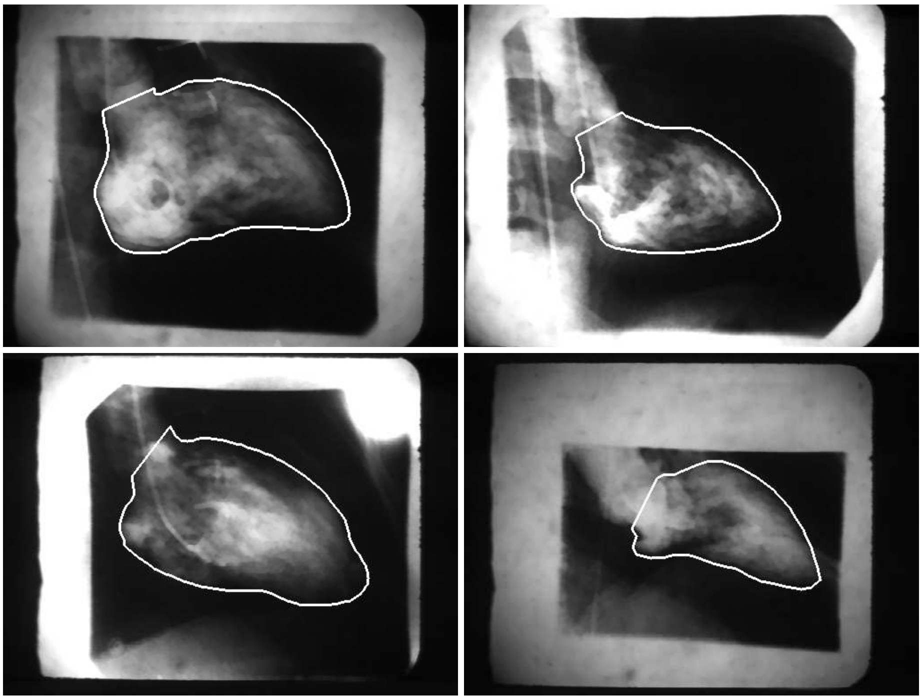

scale image is even harder to estimate compared to the end diastole apex position because the contrast level is further decreased in the apex zone in the end systole frame of the cardiac cycle.

3 Pre-Processing of Gray scale Cardiac Data

The pre-processing of the cardiac gray scale data consists of: (i) Morphological smoothing and (ii) Heart rate normalization.

3.1 Morphological smoothing

The first step is gray scale morphological smoothing which consists of a gray scale opening followed by a gray scale closing using a disk structuring element. Gray scale opening and closing [12] are defined in an analogous way to opening and closing in binary morphology. They have the similar properties. First, the definitions of gray scale dilation and erosion are defined followed by the gray scale opening and closing.

Fig. 4. ES frames for different patient studies showing the variability in the LV shape, size, position and orientation. LVG size: 384 x 512. **Top Left**: Bulge seen in the anterior wall and sharp bends in the inferior wall. **Top Right**: Bulge in the inferior wall. **Bottom Left**: Unusually large left ventricle for the ES frame. **Bottom Right**: Inferior wall deshaped like a cusp.

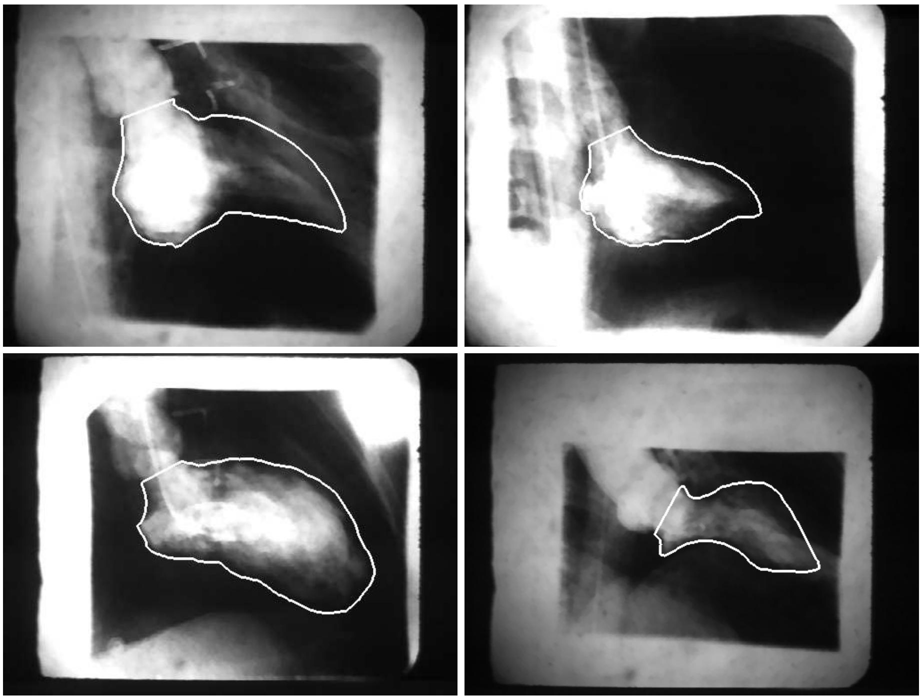

Dilation If f: F→E and k:K→E, the dilation of f by k is denoted by $f \oplus k$ and is define by:

$$f \oplus k = max_{z \in k}\{f(x-z) + k(z) | x - z \in F\} \tag{1}$$

Erosion If f: F→E and k:K→E, the erosion, $f \ominus k$ and is define by:

$$f \ominus k = min_{z \in k}\{f(x+z) - k(z) | z \in k\} \tag{2}$$

Opening If f: F→E and k:K→E, then the gray scale opening of f by a structuring element k is denoted by

$$f \circ k = (f \ominus k) \oplus k. \tag{3}$$

$$(f \circ k)(x) = max_{z \in k}\, min_{y \in k}\{f(x - z + y)\} \tag{4}$$

Fig. 5. Demonstration of the variability of the gray scale contrast data of a patient study during the systole cycle (contraction phase). Shown are the normalized frames of size 384 x 512 pixels. These images are obtained from the raw left ventricle images of size 480 x 512 after gray scale normalization, scaling, and morphological smoothing.

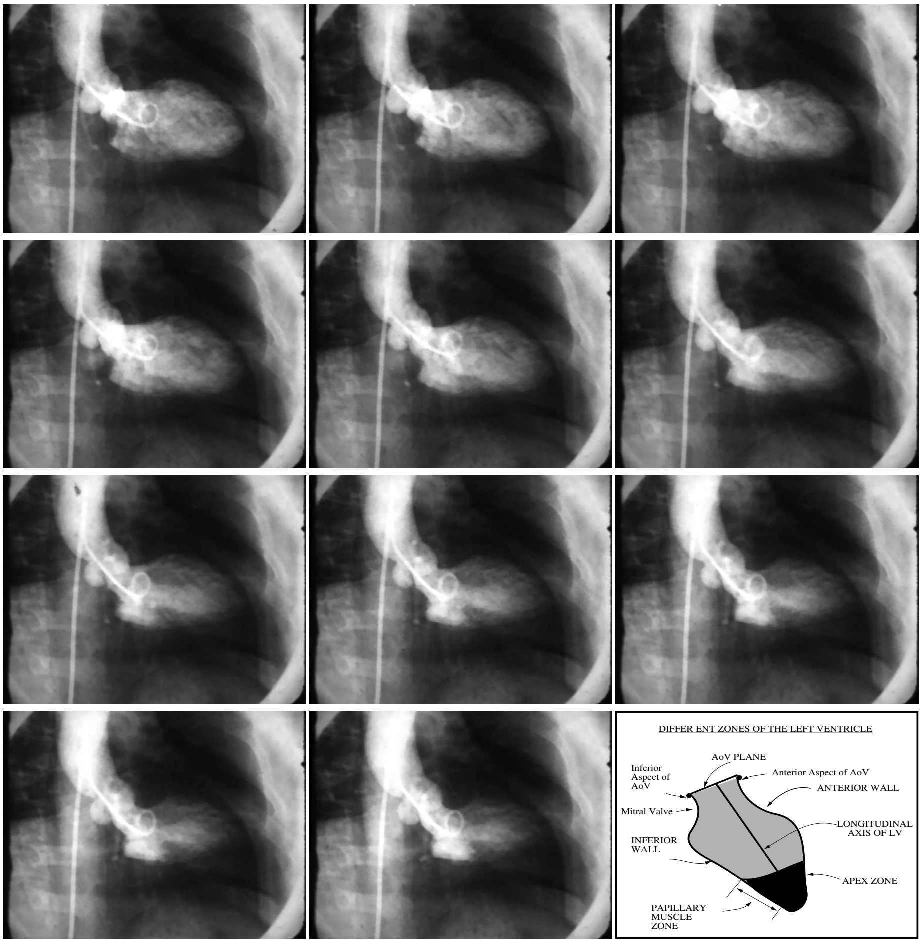

It can also be understood in terms of Umbras as:

$$f \ominus k = T[U[f] \ominus U[k]] \tag{5}$$

where, U[f] is the umbra of surface f, U[k] is the umbra of the surface k, and T is the transformation operator. Opening basically smooths contours, breaks isthmuses, eliminates small islands or peninsulas and eliminates sharp peaks.

Closing Closing basically smooths contours, fuses narrow breaks, fuses long bulfs, eliminates small holes and fills gaps. If f: F→E and k:K→E, then the gray

Fig. 6. Left: Anterior and inferior wall do not have uniform motion when moved from end diastole to end systole boundary. **Right**: Anterior wall has not moved much from end diastole to end systole boundary.

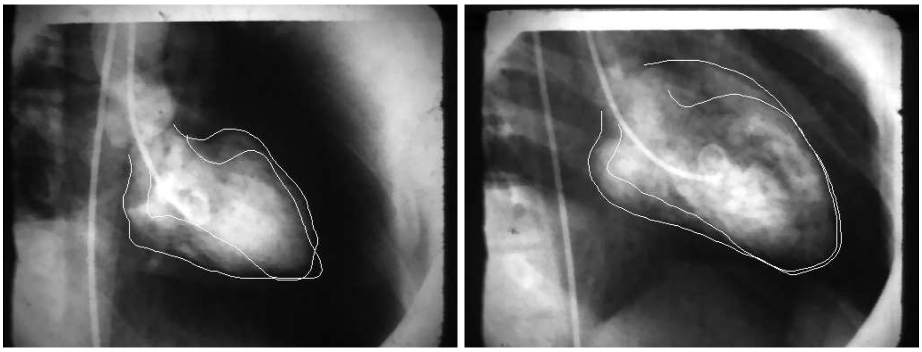

scale closing of f by a structuring element k is denoted by

$$f \bullet k = (f \oplus k) \ominus k. \tag{6}$$

This can also given in the discrete case as:

$$(f \bullet k)(x) = min_{z \in k}\, max_{y \in k}\{f(x + z - y)\} \tag{7}$$

If f: F→E and k:K→E, then $f \oplus k$ =F ⊕ K → E. It can also be understood in terms of Umbras as under:

$$f \ominus k = T[U[f] \ominus U[k]] \tag{8}$$

In terms of Umbras, the erosion of f by k is by taking the surface of the erosion of the Umbra of f by the Umbra of k.

3.2 Interpretation of the Opening and Closing

Opening and closing was explained by Sternberg [12] using a physical picture of the gray scale opening and closing of the rolling ball algorithm. In this algorithm, the closing of the gray scale image $a(x, y)$ by a spherical structuring element S is visualized in terms of the closing of the Umbra $U[a]$ by S. Imagine an extra terrestrial landscape of peaks and valleys and visualize a sphere which is free to move above the terrain surface but whose downward mobility is constrained by the surface. The closing is formed by the union of all translations of the sphere above and touching the gray scale surface. Sternberg calls it a rolling ball because those that touch the surface are said to be rolling on the surface. Closing a gray scale surface by dilating and then eroding by a spherical structuring elements rolls the ball. Gray scale opening by a spherical structuring element is visualized as a ball rolling along the underside of the gray level surface. The effect of the opening is opposite to that of closing. Ruts and pits are followed while peaks and ridges leave gaps in the coverage of the rolling ball.

3.3 Heart Rate Normalization

Stage two of the pre-processing consists of a gray scale heart normalization that normalizes the variable number of frames to a fixed number of frames (30). From the ground truth database the average ratio of the total frames in diastole cycle to the total number of frames in the cardiac cycle is:

$$r_d = \frac{n_{ED}}{n_{ED} + n_{ES}} \tag{9}$$

This ratio r_d is 0.4. Thus the systole cycle consists of 0.4 $\times$ 30=12 frames and the diastole cycle consists of 0.6 $\times$ 30=18 frames. The interpolation is made from the variable number of frames (F_v) to 30. If a patient study has F_v variable number of frames, then there are $0.4F_v$ frames in systole cycle and $0.6F_v$ frames in diastole cycle. Thus the interpolation is done from $0.4F_v$ to 12 frames for systole cycle and $0.6F_v$ frames to 18 frames in diastole cycle. First and the last frame's gray scale values are fixed thus interpolation is applied to $F_v - 2$ frames. Interpolation is done in the following way. A sequence of gray scale values at a fixed location throughout the cardiac cycle of F frames, $g_i, i = 1, \ldots, F$, is extracted. The number of frames in systole F_s and that in diastole F_d are $0.4F_v$ and $0.6F_v$. For the sequence of $F_s(F_d)$ frames, we interpolate it into a sequence of 12(18) frames. Let us assume F_i frames are interpolated into F_I. The last stage of the pre-processing consists of normalization of the gray scale intensities between 0 to 255.

4 Bayesian Approach to Pixel Classification

Lee et al. [1] developed a classical Bayesian classification framework for solving the left ventricle boundary detection problem. From the multiple LVG's throughout the cardiac cycle and the corresponding ground truth which are manually traced boundaries, the *a priori* probability for any position (x, y) being in any class c was estimated. This *a priori* probability is also made dependent of the user input of 3 points: the aortic valve plane (2 points) and the apex (1 point).

A pixel's class label c means that the pixel is in LV from the first frame to frame $(c-1)$ and out of LV from frame c to the end systolic frame in systole and *vice versa* in diastole. This class assignment strategy enables us to transform the classifier result to a sequence of 0's and 1's, which results in an LV region at each frame. Note, heart rate normalization was done to fix the length of the feature vector.

Lee made two assumptions in classifying the pixels from the multiple frames of the LVG. The first one is that the end-systolic frame number from a new patient's LVG is known prior to the classification step. This permitted Lee to deal with the frames in the systole cycle and those in diastole separately. Another assumption was with respect to the heart motion. The heart motion is mainly contracting in systole and expanding in diastole. This means that when we look at a pixel location throughout the cardiac cycle, there is at most one transition in

Fig. 7. From a binary sequence, class number is decided.

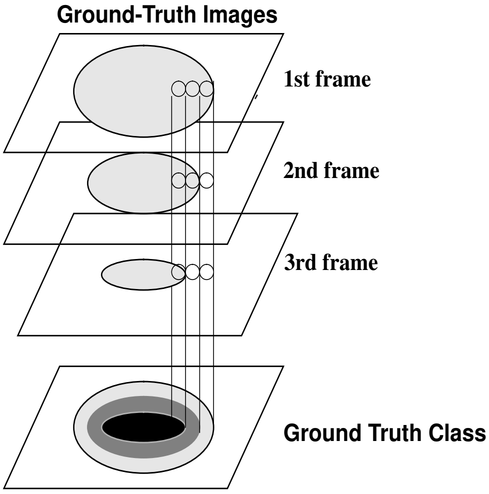

systole where the location is in left ventricle and then moves out of LV. Likewise there is at most one transition in diastole where the location out of LV moves inside LV.

4.1 Problem Statement

Under Lee's restricted motion assumptions, the problem statement can be formulated as a problem of maximizing the expected gain using a restricted set of classes.

> Given F_s grey-scale images in systole, $G_i, i = 1, \ldots, F_s$,
> Classify a pixel at location (x, y) and having gray values $(g_1, \ldots, g_{F_s})$ to class $c \in \{1, 2, \ldots, F_s, F_s + 1\}$ where c which maximizes
>
> $$\sum_{c'} e(c, c')P(c'|X)$$
>
> where $(g_1, \ldots, g_{F_s})$ is the feature vector X, $P(c|X) = P(X|c)P(c)/P(X)$ and $P(X|c)$ is class conditional probability and $P(c)$ is the *a priori* class probability which depends on image position.

4.2 Ground Truth Class Assignment

The ideal class assignment was determined from the physician's hand-drawn boundaries of the LV region in each frame. Filling the inside of these boundaries by pixel value "1" produces *LV regions*, $\bar{R}_f$, $f = 1, \ldots, F_s(F_d)$. A location in region $\bar{R}_f$ means that the location is in the LV at frame i. By stacking LV regions of the entire cardiac cycle, $\bar{R}'_f s$, we can look at them as 3 dimensional array

Table 3.2. Binary sequence pattern under the monotonic motion assumption.

frame	Diastole			
1	1 0 0 $\cdots$	0	0	0
2	1 1 0 $\cdots$	0	0	0
3	1 1 1 $\cdots$	0	0	0
$\vdots$		$\vdots$		
F_d	1 1 1 $\cdots$	1	0	0
F_d	1 1 1 $\cdots$	1	1	0
class number	1 2 3 $\cdots$	$F_d - 1$	F_d	$F_d + 1$

(a) Diastole.

frame	Systole			
1	0 1 1 $\cdots$	1	1	1
2	0 0 1 $\cdots$	1	1	1
3	0 0 0 $\cdots$	1	1	1
$\vdots$		$\vdots$		
$F_s - 1$	0 0 0 $\cdots$	0	1	1
F_s	0 0 0 $\cdots$	0	0	1
class number	1 2 3 $\cdots$	$F_s - 1$	F_s	$F_s + 1$

(b) Systole.

specified by frame number, row coordinate, and column coordinate, (f, x, y). For any location specified by (x, y), we can extract the sequence of 0's and 1's, from which the class number for that location can be estimated (see Figure 7).

In systole (diastole) of $F_s(F_d)$ frames, the number of all possible sequences is $2^{F_s}(2^{F_d})$, but that of realistically feasible sequences is far less. Under the assumption we made about the LV motion, contracting in systole and expanding in diastole, the ideal sequence has the following patterns (Table 3.2) and the number of cases is $F_s(F_d) + 1$.

But the ground truth sequences from the LV regions differ from the ideal ones in that they include multiple 1-0 transitions and 0-1 transitions. The ground truth class is, therefore, determined by a matched filter. From the sequence of 0's and 1's, $< b_1, b_2, \ldots, b_F >$, we determine its ground truth class by applying a matched filter with the kernel 11000 in systole and the kernel 00111 in diastole. These kernels were choosen based on the monotonic LV boundary motion assumption. Prior to the matched filter, a running average filter of length 5 is applied. The matched filter with the kernel picked the frame number at which the transition occurs. If there is more than one transition that occurs in the sequence, it picks the first one. If the sequence is all 1's (0's) in systole (diastole), the class number is $F_s(F_d)+1$ and if the sequence is all 0's (1's), the class number is 1. Figure 8. shows Ground-truth class image for systole and for diastole.

4.3 Class To Sequence To LV Region Mapping

In the assignment of ground truth to each pixel location we convert the binary sequence to a class label. We also need its inverse operation which converts a class label into a sequence of 0's and 1's where 0 means out of LV and 1 means in LV. Under the monotonicity motion assumption, class c in systole means that the transition from 1 to 0 occurs at the c-th frame, *i.e.*, the location is in the region up to frame $c - 1$ and out of the region from frame c. The conversion of a pixel's class label c to the corresponding binary sequence $< b_1, \ldots, b_F >$ is accomplished by defining

$$\begin{cases} b_n = 1 \text{ if } n < c \\ b_n = 0 \text{ otherwise} \end{cases}$$

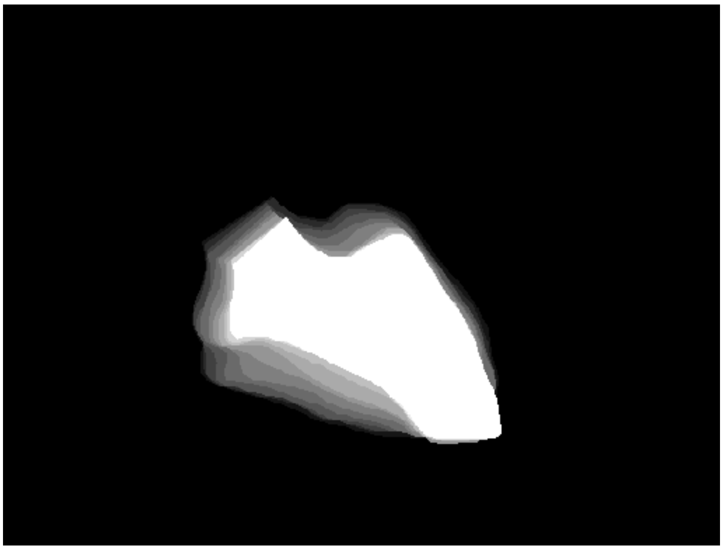

(a) Systole, class number increases from 1 to 13 as the pixel becomes brighter.

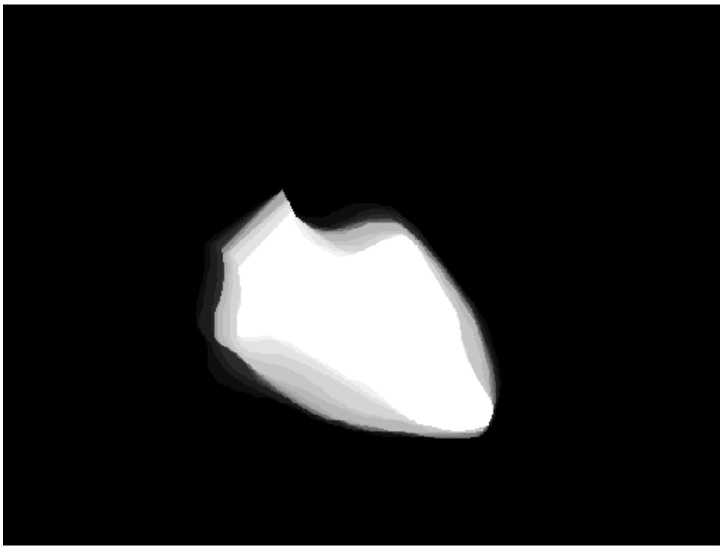

(b) Diastole, class number increases from 1 to 18 as the pixel becomes darker.

Fig. 8. Ground truth class images for systole and diastole. Class number represents the frame number of the pixel's transition from inside to outside (systole) of the heart and from outside to inside (diastole) due to the compression and the expansion.

Fig. 9. Conversion of class label to the corresponding binary sequence.

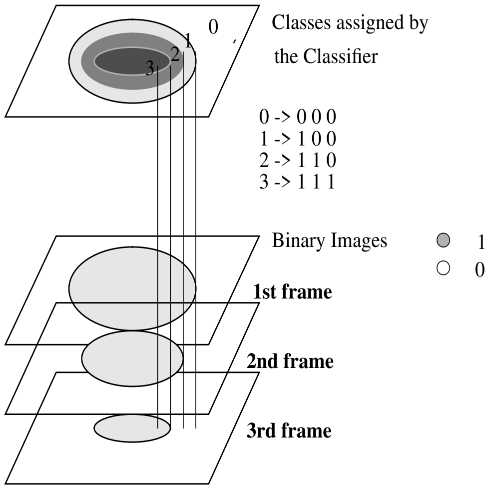

and is shown in Figure 9.

Elements of the sequences of all locations for a fixed frame tells us whether each location is in LV or out of LV. At each frame, the region made up of all the pixels in LV is called by *observed LV region* R_i, and is defined by

$$R_i = \{(x, y) \mid C(x, y) \geq c\}$$

where $c = 1, \ldots, F_s + 1$ and $C(x, y)$ denotes class label assigned to location (x, y). *Observed LV regions* are found for all frames simultaneously. Figure 10. is the multiband image generated from the ground truth class image of Figure 7.

4.4 Maximum Expected Economic Gain Classifier

Each pixel is specified by patient i, frame number f, x-coordinate x, and y-coordinate y. Its gray-value is $g(i, f, x, y)$. From the hand-drawn boundary associated with the LVG, we obtain the corresponding LV region by filling the inside of the boundary. The indicator function for the LV region is denoted by $r(i, f, x, y)$ and is defined by

$$r(i, f, x, y) = \begin{cases} 1 \text{ if } (i, f, x, y) \text{ is in LV Region} \\ 0 \text{ otherwise} \end{cases}$$

where $1 \leq i \leq F_p$, $1 \leq f \leq F$, $1 \leq x \leq IX$, and $1 \leq y \leq IY$. IX and IY are the number of rows and number of columns in the image. The ground truth class number $C(i, x, y)$ at location (x, y) for patient i is extracted from the sequence $< r(i, 1, x, y), \ldots, r(i, F_s, x, y) >$.

We initially assumed that the feature vector of patient i, $X(i, x, y)$, consisting of grey values at location (x, y) of all frames, $g(i, f, x, y)$, $f = 1, 2, \ldots, F_s$, follows

Fig. 10. Multiband images generated by class to sequence mapping from ground-truth class image. 12 frames for systole and 18 frames for diastole.

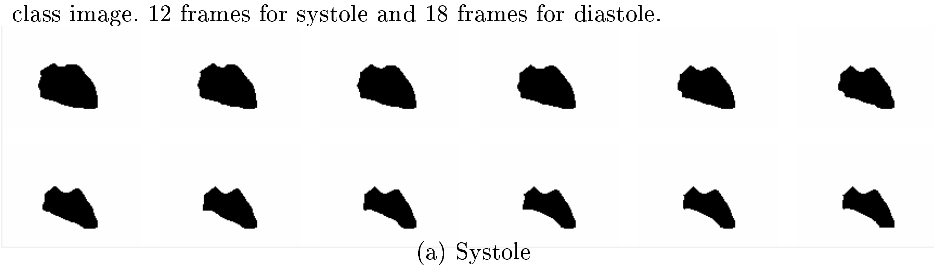

(a) Systole

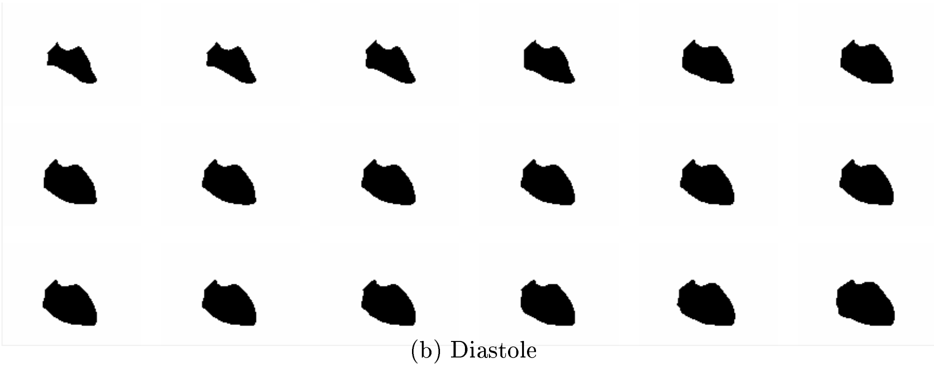

(b) Diastole

a multi-variate normal distribution which is specified by

$$P(X|c) = P(X|\mu_c, \Sigma_c) = (2\pi)^{-\frac{F_s}{2}} |\Sigma_c|^{-\frac{1}{2}} \exp(-\frac{1}{2}(X - \mu_c)^t \Sigma_c^{-1} (X - \mu_c))$$

Then we refined this model by determining from the training data for each class c the histogram $h(*; c)$ of

$$(X - \mu_c)^t \Sigma_c^{-1} (X - \mu_c)$$

for all X in class c and used

$$P(c|x) = h((X - \mu_c)^t \Sigma_c^{-1} (X - \mu_c); c)$$

With this model, our problem statement becomes

> For a given feature vector X find the class c which maximizes the expected gain
> $$\sum_{c'} e(c, c') P(c'|X)$$

where $e(c, c')$ is the economic gain for assigning class c when class c' is the true class.

Parameter Estimation From the training data set, we can estimate the mean vector $\hat{\mu}_c$ and the covariance matrix $\hat{\Sigma}_c$ for each class. The estimated class mean and covariance matrix specify the class probability distribution $P(X|\hat{\mu}_c, \hat{\Sigma}_c)$. Mean vector and covariance matrix for class c are estimated by

$$\hat{\mu}_c = \frac{1}{\#L_c} \sum_{(i,x,y)\in L_c} X(i,x,y)$$

$$\hat{\Sigma}_c = \frac{1}{\#L_c - 1} \sum_{(i,x,y)\in L_c} (X(i,x,y) - \hat{\mu}_c)\,(X(i,x,y) - \hat{\mu}_c)^t$$

where

$$L_c = \{(i,x,y)|C(i,x,y) = c\}$$

In order to reduce the number of parameters to estimate, the pooled covariance matrix is used, which is estimated by

$$\hat{\Sigma} = \frac{\sum_{c=1}^{F_c} L_c \hat{\Sigma}_c}{\sum_{c=1}^{F_c} L_c}$$

Once a classified image is computed, it is spatially simplified and the boundary of the largest connected component on the simplified image is determined. We call this boundary the raw classified boundary. Fig. 11 shows a typical raw classification boundary for the end diastole and end systole frames of the cardiac cycle.

5 Systematic Error Cancellation

The raw boundaries obtained from the pixel classifier have significant error and much of the error in the inferior wall and apical zone is systematic and can be eliminated with a post-processing procedure that uses physician specified points for the aortic valve plane and the apex.

5.1 Calibration methodology

The systematic boundary error cancellation methodology is, in effect, a calibration procedure which calibrates out all systematic position, orientation, and shape errors of the raw classified boundaries. The calibration transformation is estimated using a database consisting of the ground truth boundaries and the corresponding raw boundaries generated by the classifier [1]. The cross-validation protocol for estimating the accuracy of the boundary error cancellation procedure takes a database of N patient studies and partitions it into K equal sized subsets. Then for all K *choose* L combinations, the transformation using L subsets is estimated. Now using the estimated transformation on the remaining $K - L$ subsets, the mean error of the transformed boundary is estimated.

Fig. 11. Results of the pixel classification algorithm over ED and ES frames of the cardiac cycle. **Top row**: End Systole (ES) frame showing very little dye in the apex zone of the left ventricle and the pixel classification boundary (the thin boundary line) falls short in the apical zone. Also seen is the over estimation of the inferior walls. Thicker boundaries are the boundaries drawn by the cardiologist. **Bottom row**: End-Diastole (ED) frame showing very little dye in the apex zone of the left ventricle and the pixel classification boundary (the thin boundary line) is under-estimated in the apex zone of the left ventricle. The thick boundary lines represent the boundary of the left ventricle as delineated by the cardiologist.

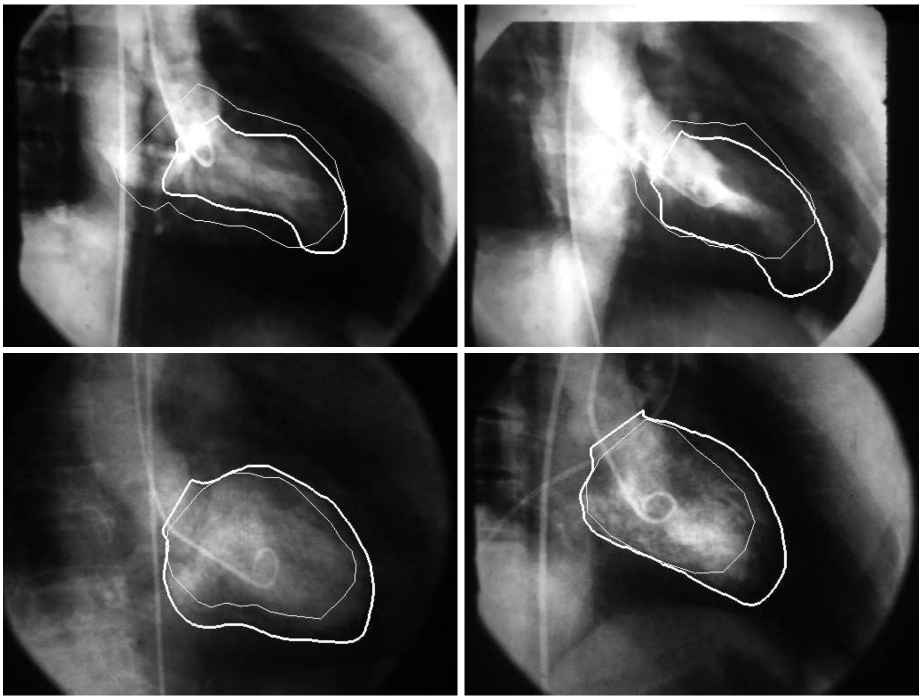

5.2 Sampling

The input raw and ground truth boundaries are initially in an irregularly spaced vertex polygon format with 100 vertices and unit dimensions in millimeters. The polygons are resampled and interpolated into into an appropriate number of equally spaced vertices before it undergoes the calibration procedure discussed below.

5.3 Performance and data analysis scheme

The error between a computed boundary and the ground truth boundary is defined as the average distance between each vertex of the computed boundary and the polygon of the ground truth boundary and the distance between each vertex of the ground truth boundary and the polygon of the computed boundary.

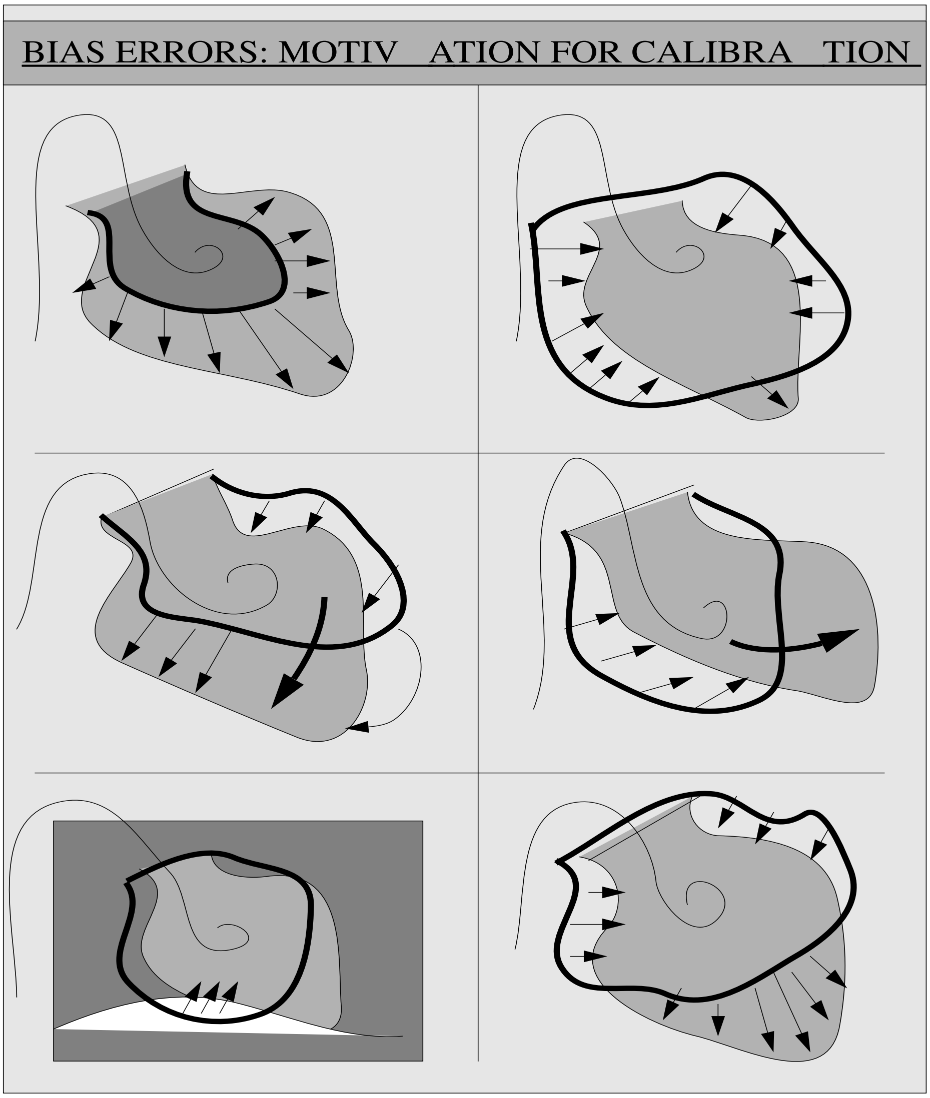

Fig. 12. Bias errors produced by the pixel classification system. **Top row**, left and right: classifier boundary inside and outside the ideal boundary. **Middle row**,left and right: classifier boundary towards the anterior and inferior wall. **Last row**,left: classifier boundary overlaps the diaphragm. **Last row, right**: classifier boundary outside the ideal boundary in top two-third region and under-estimated in the bottom one-third region.

For each vertex of the boundary, the calibrated x-coordinate is computed as the linear combination of raw x- *and* raw y-coordinates of the left ventricle boundary and the x and y coordinate of the three user entered points in all possible combinations up to 2nd order terms: this constitutes 1 zero order term, 6 first order terms, and 21 second order terms. The coefficients associated with the linear combination change for each vertex. And the values of the coefficients are estimated by a least squares regression. The calibrated y-coordinate of that vertex is computed with a *different* linear combination of raw x- *and* y-coordinates and the 2nd order terms of the three user-entered points.

5.4 The Least Squares Regression Problem Setup

Let $g_n^{'}$ and $h_n^{'}$ be the row vectors of x- and y-coordinates for any patient n. Let $r_n^{'}$ and $s_n^{'}$ be the row vectors of x- and y-coordinates of the classifier boundary. For the calibrated boundary estimation in ventriculograms using the *independent coefficient* method, we are:

- **Given**: Corresponding ground truth boundaries $\mathbf{R}$ $[N \times 2P]$, classifier boundaries $\mathbf{Q}$ $[N \times (2P + 28)]$ respectively:

$$\mathbf{R} = \begin{pmatrix} g_1^{'} \; h_1^{'} \\ \ldots \\ g_N^{'} \; h_N^{'} \end{pmatrix} \quad \mathbf{Q} = \begin{pmatrix} r_1^{'} \, s_1^{'} \, t_1^{'} \\ \ldots \\ r_N^{'} \, s_N^{'} \, t_N^{'} \end{pmatrix}$$

  where, $t_1^{'}$ are the 1+6+21 augmented terms coming from the 3 user input points of the first study and $t_N^{'}$ is the 1+6+21 augmented terms coming from the 3 user input points of the N^{th} study.

- Let $\mathbf{A}$ $[(2P + 28) \times 2P]$ be unknown regression coefficient matrix.
- The problem is to estimate the coefficient matrix $\mathbf{A}$ and to minimize $\| \mathbf{R} - \mathbf{Q}\,\mathbf{A} \|^2$. Then for any classifier boundary matrix $\mathbf{Q}$, the calibrated vertices of the boundary are given by $\mathbf{Q}\hat{\mathbf{A}}$, where $\hat{\mathbf{A}}$ is the estimated coefficients.

This problem is solved by the standard least squares solution.

Due to the finite number of our patient studies, 377, and the large number of coefficients being estimated, there is a relationship between the number of vertices we sample the polygon and the resulting mean and standard deviation of the boundary error on the test set. If we sample to many points, we in effect memorize the training data and performance on the test set will be poor. If we sample to few points, we do well in terms of generalizing but we incur a large error due to the coarse sampling. Therefore we optimize for the number of vertices. At the optimal values the mean boundary error is just more than 2.4 millimeters.

Fig. 13. Classifier vs. Estimated boundaries with gray scale in the back ground using the systematic error cancellation procedure patient name: **1017f**, **Thick LV contour** -Ground Truth, **Thin LV contour**-Classifier, and Estimated, **Upper**: (a1) Classifier ED frame boundary with ground truth. (a2) Calibrated ED frame boundary with ground truth. **Bottom**: (b1) Classifier ES frame boundary with ground truth. (b2) Calibrated ES frame boundary with ground truth. Mean end frame error $(\frac{ED+ES}{2}) =$ 2.0 mm,

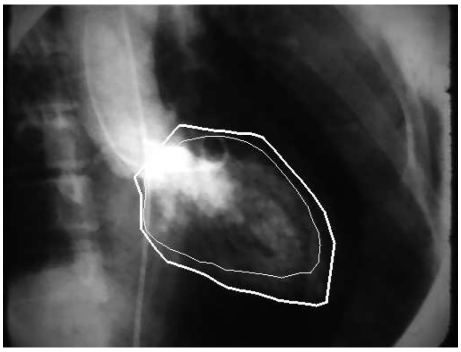

(a1) ED Frame: GT and Classifier

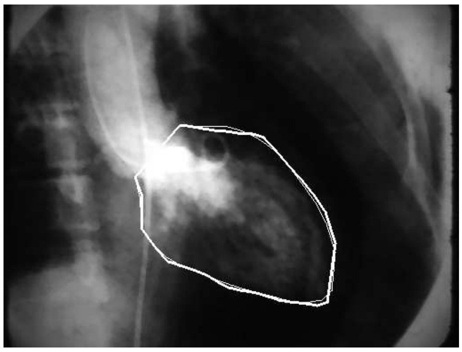

(a2) ED Frame: GT and Estimated

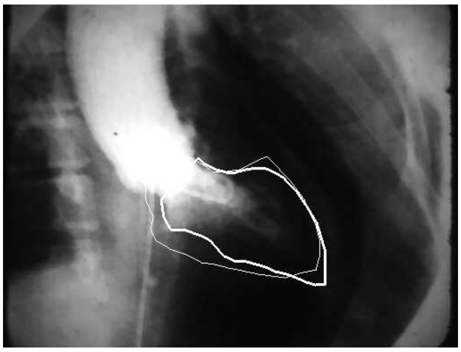

(b1) ES Frame: GT and Classifier

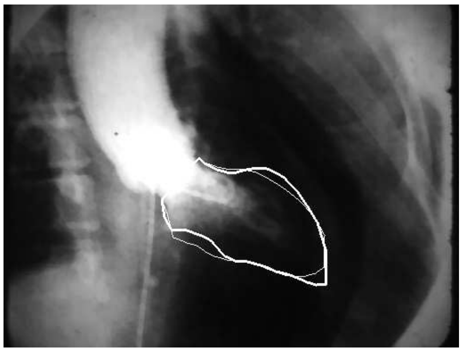

(b2) ES Frame: GT and Estimated

6 Future Work

We are currently examining the errors produced by the algorithm in an attempt to refine it to reduce the average error to less than 2mm. Then we will gather statistics on the ejection fraction estimates that are based on the automatic boundary delineation algorithm.

References

1. C. K. Lee, *Automated Boundary Tracing Using Temporal Information*, Ph.D Thesis, Department of Electrical Engineering, Universtiy of Washington, Seattle, 1994.

2. Helmut Wollschleger, Robert Wal Tenspiel, Ulrich Solzbach, Andreas M. Zeiher and Hangoerg Just, *Reliable Automatic Frame-By-Frame Contour Detection of Digitized LV Cine-Angiograms*, IEEE Computers in Cardiology, p353-p356, 1988.
3. Florence H. Sheehan, Robert M. Haralick, Jasjit S. Suri and Yong Shao, *Method for determining the contour of an In Vivo Organ Using Multiple Image Frames of the Organ*, Contents: (i) Aorta and the Aortic Valve Plane Estimation (ii) Left ventricle boundary estimation, Patent Submitted to University of Washington, Seattle, filed through Office of Technology Transfer (OTT), File Number 1221, August 1996.
4. Jasjit S. Suri, Robert M. Haralick and F. H. Sheehan, *Two Automatic Calibration Algorithms for Left Ventricle Boundary Estimation in X-ray Images*, Published in Proc. of IEEE Int. Conf. of Engineering in Medicine and Biology (EMBS), Amsterdam, The Netherlands, ISBN 90-9010005-9(CD-ROM) SOE 9609001, Oct 31 - Nov. 3, 1996.
5. Jasjit S. Suri, Robert M. Haralick and F. H. Sheehan, *Two Calibration Algorithms and Its Performance for Boundary Estimation of Left Ventricle in Noisy Ventriclograms*, Accepted for Jour. of IEEE Trans. in Bio Engineering, 1996, revision required.
6. Jasjit S. Suri and Robert M. Haralick, *Systematic Error Correction in automatically produced boundaries in Low Contrast Ventriculograms*, International Conference in Pattern Recognition, Austria, 1996.
7. Jasjit S. Suri, Robert M. Haralick and F. H. Sheehan, *Correction of Systematic Errors in Automatically Produced Boundaries from Low Contrast Ventriculograms*, Accepted (final submission) for Journal of IEEE Trans. in Medical Imaging, 1996.
8. Jasjit S. Suri, Robert M. Haralick and Florence H. Sheehan, *Accurate Left Ventricle Apex Position and Boundary Estimation From Noisy Ventriculograms*, Proceedings of the IEEE Computers in Cardiology, Indianapolis, 1996.
9. Jasjit S. Suri, Robert M. Haralick and F. H. Sheehan, *A General technique for automatic Left Ventricle Boundary Validation: Relation Between Cardioangiograms and Observed Boundary Errors*, Accepted for: Society for Computer Applications in Radiology (SCAR), Rochester, Minnesota, June 21-24, 1997.
10. Jasjit S. Suri, Robert M. Haralick and F. H. Sheehan, *Effect of Edge Detection, Pixel Classification, Classification-Edge Fusion Over LV Calibration, A two Stage Automatic system, 10th Scandinavian Conference on Image Analysis (SCIA '97)*, June 9-11, Finland, 1997.
11. Jasjit S. Suri, Robert M. Haralick and F. H. Sheehan, *Abstract: Accurate Left Ventricle Position and Boundary Estimation from Noisy Ventriculograms*, Computers in Cardiology 1996, Indianapolis, page 68, S52.1, Left Ventricular Wall Motion Track, Sep. 8-11, 1996, Indiana, USA.
12. Sternberg, *Grayscale Morphology*, Computer Vision, Graphics, Image Processing, 1985.